

1 **Measurement Report: Effects of anthropogenic emissions and**
2 **environmental factors on biogenic secondary organic aerosol**
3 **(BSOA) formation in a coastal city of Southeastern China**

4

5 Youwei Hong^{a,b,c,d*}, Xinbei Xu^{a,b,c}, Dan Liao^e, Taotao Liu^{a,b,c}, Xiaoting Ji^{a,b,c}, Ke Xu^{a,b,d},
6 Chunyang Liao^f, Ting Wang^g, Chunshui Lin^g, Jinsheng Chen^{a,b,c*}

7

8 ^aCenter for Excellence in Regional Atmospheric Environment, Institute of Urban Environment,
9 Chinese Academy of Sciences, Xiamen, 361021, China

10 ^bKey Lab of Urban Environment and Health, Institute of Urban Environment, Chinese Academy
11 of Sciences, Xiamen, 361021, China

12 ^cUniversity of Chinese Academy of Sciences, Beijing, 100049, China

13 ^dSchool of Life Sciences, Hebei University, Baoding, 071000, China

14 ^eCollege of Environment and Public Health, Xiamen Huaxia University, Xiamen 361024, China

15 ^fState Key Laboratory of Environmental Chemistry and Ecotoxicology, Research Center for Eco-
16 Environmental Sciences, Chinese Academy of Sciences, Beijing 100085, China

17 ^gInstitute of Earth Environment, Chinese Academy of Sciences, Xi'an, 710061, China

18

19 *Corresponding author E-mail: Jinsheng Chen (jschen@iue.ac.cn); Youwei Hong
20 (ywhong@iue.ac.cn)

21

22

23

24

25

26

27

28

29

30

31

32

33

34 **Abstract:**

35 To better understand the formation of biogenic secondary organic aerosol (BSOA),
36 aerosol samples with a 4 h time resolution were collected during summer and
37 wintertime in the southeast of China, along with on-line measurements of trace gases,
38 aerosol chemical compositions, and meteorological parameters. The samples were
39 analyzed by gas chromatography-mass spectrometry for PM_{2.5}-bound SOA tracers,
40 including isoprene (SOA_I), α/β -pinene (SOA_M), β -caryophyllene (SOA_C), and toluene
41 (ASOA). The average concentrations of total SOA tracers in winter and summer were
42 38.8 and 111.9 ng m⁻³, respectively, with the predominance of SOA_M (70.1% and
43 45.8%), followed by SOA_I (14.0% and 45.6%), ASOA (11.0% and 6.2%) and SOA_C
44 (4.9% and 2.3%). Compared to those in winter, the majority of BSOA tracers in summer
45 showed significant positive correlations with Ox (O₃+NO₂) ($r = 0.443 \sim 0.808$), HONO
46 ($r = 0.299 \sim 0.601$), ultraviolet (UV) ($r = 0.382 \sim 0.588$) and temperature (T) ($r =$
47 $0.529 \sim 0.852$), indicating the influence of photochemical oxidation under relatively
48 clean conditions. However, in winter, BSOA tracers were significantly correlated with
49 PM_{2.5} ($r = 0.407 \sim 0.867$), NO₃⁻ ($r = 0.416 \sim 0.884$), SO₄²⁻ ($r = 0.419 \sim 0.813$), and NH₃
50 ($r = 0.440 \sim 0.757$), attributed to the contributions of anthropogenic emissions. Major
51 BSOA tracers in both seasons was linearly correlated with aerosol acidity (pH) ($r =$
52 $0.421 \sim 0.752$), liquid water content (LWC) ($r = 0.403 \sim 0.876$) and SO₄²⁻ ($r = 0.419 \sim$
53 0.813). The results indicated that acid-catalyzed reactive uptake onto sulfate aerosol
54 particles enhanced the formation of BSOA. In summer, the clean air mass originated
55 from the ocean, and chlorine depletion was observed. We also found that concentrations
56 of the total SOA tracers was correlated with HCl ($R^2 = 0.545$) and chlorine ions ($r =$
57 $0.280 \sim 0.639$) in PM_{2.5}, reflecting the contribution of Cl-initiated VOC oxidations to
58 the formation of SOA. In winter, the northeast dominant wind direction brought
59 continental polluted air mass to the monitoring site, affecting the transformation of
60 BSOA tracers. This implied that anthropogenic emissions, atmospheric oxidation
61 capacity and halogen chemistry have significant effects on the formation of BSOA in
62 the southeast coastal area.

63 **Keywords:** SOA tracers; biogenic volatile organic compounds; anthropogenic
64 pollutants; atmospheric oxidation capacity; coastal area
65

66 **1. Introduction**

67 Secondary organic aerosol (SOA) has attracted widespread scientific research
68 concerns, due to its potential impacts on climate change, human health and air quality
69 (Shrivastava et al., 2017; Reid et al., 2018; Zhu et al., 2019; Wang et al., 2021b).
70 Understanding the formation of SOA and assessing its relevance for environmental
71 effects become an integral part of aerosol chemistry (Charan et al., 2019; Xiao et al.,
72 2020; Palmer et al., 2022). However, due to its complex precursors and atmospheric
73 physical or chemical processes, SOA prediction by air quality models remains highly
74 uncertain (McFiggans et al., 2019). Therefore, it is necessary to better explore missed
75 SOA sources and unknown SOA formation mechanisms.

76 SOA is produced by the conversion of biogenic and anthropogenic volatile organic
77 compounds (BVOCs and AVOCs) through complex homogeneous and heterogeneous
78 reactions (Charan et al., 2019; Xiao et al., 2020; Mahilang et al., 2021). BVOCs are the
79 main precursors of SOA on a global scale, while AVOCs are the predominant
80 contributor to SOA in urban areas (Hallquist et al., 2009; Wang et al., 2021a). Recently,
81 laboratory, field and modeling studies have shown that anthropogenic emissions greatly
82 affect the formation of BSOA (Hoyle et al., 2011; Shrivastava et al., 2019; Zhang et al.,
83 2019b; Zhang et al., 2019c; Mahilang et al., 2021; Xu et al., 2021). Anthropogenic air
84 pollutants, such as NO_x, SO₂, NH₃ and aerosols, could influence the conversion of
85 BVOCs to the particulate phase and the production of nitrogen and sulfur compounds
86 (Wang et al., 2020). NO_x is one of the important drivers of SOA formation and yields
87 during both daytime and nighttime through alternating the fate of peroxy radicals (RO₂·)
88 (Sarrafzadeh et al., 2016; Newland et al., 2021). While ·OH dominates the
89 photochemical oxidation of BVOC during daylight hours, and NO₃· becomes one of the
90 main oxidants for biogenic SOA and organic nitrate formation at night. SO₂ also plays

91 an important role in changing SOA formation from BVOC photooxidation and
92 ozonolysis through sulfuric acid formation and acid-catalyzed heterogeneous reactions
93 (Zhao et al., 2018; Zhang et al., 2019b; Xu et al., 2021). In addition, NH₃ and amines
94 can affect the SOA yields and composition through both gas-phase and heterogeneous
95 reactions, by reacting with sulfuric or nitric acid to generate secondary inorganic
96 aerosols (SIA) (Ma et al., 2018; Liu et al., 2021; Lv et al., 2022). However, due to
97 complex precursors and atmospheric processes, the combined effects of anthropogenic
98 emissions and meteorological factors on the formation of SOA are not fully understood.

99 The coastal area of southeastern China is under the East Asian monsoon control,
100 which cause an obvious alternation of polluted and clean air masses from continental
101 and ocean area, respectively (Wu et al., 2019; Hong et al., 2021). Also, the local
102 geographical environment, including relatively high humidity, dense vegetation and
103 strong atmospheric oxidation capacity, provides a good chance to study the sources and
104 formation mechanisms of SOA. In our previous studies, ground-based observations in
105 a mountainous forest area of this region showed that BSOA tracers were the largest
106 contributor to SOA, and the aerosols were highly oxidized (Hong et al., 2019). However,
107 with the development of rapid urbanization, anthropogenic emissions will be of great
108 significance on SOA formation (Liu et al., 2020). Halogen radicals (chlorine, bromine,
109 iodine) have an important role in tropospheric oxidants chemistry and OA formation
110 (Wang et al., 2021c). Therefore, it is necessary to investigate the sources and formation
111 mechanisms of SOA in coastal urban areas, and so as to provide a scientific basis for
112 the estimation of regional SOA budgets and PM_{2.5} pollution control.

113 In this study, a continuous PM_{2.5} sampling campaign with a 4 h time resolution
114 was conducted in a coastal city of southeastern China during the winter and
115 summertime period. Seasonal, diurnal variations and SOC contributions of SOA tracers
116 were analyzed. Atmospheric process identified by SOA tracers in different seasons
117 were further analyzed. Finally, the combined effects of anthropogenic emissions and
118 major environmental factors on promoting SOA formation was discussed.

119 **2. Materials and methods**

120 *2.1 Sample collection*

121 The sampling was performed at the Institute of Urban Environment, Chinese
122 Academy of Sciences (118.06° E, 24.61° N), which is located in a suburban area of
123 Xiamen, a coastal city of southeastern China. Detailed information of the air monitoring
124 supersite was described in our previous study (Hong et al., 2021). Briefly, time-resolved
125 (00:00–08:00, 08:00–12:00, 12:00–16:00, 16:00–20:00, 20:00–24:00 CST – China
126 Standard Time) PM_{2.5} samples were collected on the rooftop of the station (about 70m
127 above the ground). The sampling was carried out by using a high volume (1.05 m³ min⁻¹)
128 sampler (TH-1000C, Wuhan Tianhong, China) with a PM_{2.5} inlet from 10 to 18 January,
129 and from 5 to 14 July 2020. All samples were collected onto pre-baked (450 °C, 6 h)
130 quartz fiber filters. Field blank samples were also collected. The sample filters were
131 separately sealed in aluminum foil and stored in a freezer (–20 °C) prior to analysis.

132 *2.2 SOA tracers analysis by GC/MS*

133 The isoprene-derived SOA (SOA_I) tracers included 2 methyltetrols (MTLs: 2-
134 methylthreitol (MTL1) and 2-methylerythritol (MTL2)), C5-alkene triols (cis-2-
135 methyl-1,3,4-trihydroxy-1-butene, trans-2-methyl-1,3,4-trihydroxy-1-butene, and 3-
136 methyl-2,3,4-trihydroxy-1-butene) and 2-methylglyceric acid (MGA). The
137 monoterpene-derived SOA (SOA_M) tracers were composed of pinic acid (PA), pinonic
138 acid (PNA), 3-hydroxyglutaric acid (HGA), 3-methyl-1,2,3-butanetricarboxylic acid
139 (MBTCA), 3-hydro-4,4-dimethylglutaric acid (HDMGA), and 3-acetylglutaric acid
140 (AGA). The β-caryophyllene-derived SOA (SOA_C) tracer was β-caryophyllenic acid
141 (CA), the toluene-derived SOA (SOA_A) tracer was 2,3-Dihydroxy-4-oxopentanoic acid
142 (DHOPA) and levoglucosan (LEV) as a tracer of biomass burning. Due to the lack of
143 authentic standards, surrogate standards (including erythritol, malic acid, PA and
144 citramalic acid) were used to compensate for unavoidable assay variance of SOA_I,
145 SOA_M, SOA_C and SOA_A tracer in each sample during the pretreatment process,
146 respectively (Fu et al., 2009). However, inherent low volatility of isoprene SOA tracers

147 could cause the uncertainties of using the GC/MS method, and low-volatility oligomers
148 might break down into monomers, such as C5-alkene triols and 2-methyltetrols (Lopez-
149 Hilfiker et al., 2016; Hu et al., 2016). Therefore, quantifying the abundance of certain
150 SOA tracers remained some uncertainty.

151 The analytical procedure of fifteen SOA tracers was published in our previous
152 studies (Hong et al., 2019; Liu et al., 2020). Briefly, the filter samples were
153 ultrasonically extracted with a mixture of dichloromethane and methanol (2:1, v/v) for
154 10 min three times. The mixed extracts were filtered with a PTFE filter (0.22 μm), and
155 dried with high purity N_2 (99.99%), and then derivatized with 60 μL of
156 N,O-bis-(trimethylsilyl) trifluoroacetamide (BSTFA) with 1% trimethylsilyl chloride
157 and 10 μL of pyridine at 70 $^\circ\text{C}$ for 3 h. At last, 140 μL of internal standard solution (13
158 C n-alkane solution, 1.507 $\text{ng } \mu\text{L}^{-1}$) was added into the samples. Then, relative response
159 factors (RRFs) of surrogate and internal standard were calculated to quantify the
160 targeted organic tracers in each sample. Details of SOA tracer's calculated
161 concentrations based on RRFs were presented in our previous studies (Hong et al., 2019;
162 Liu et al., 2020).

163 Fifteen SOA tracers were determined by GC-MSD (7890A/5975C, Agilent
164 Technologies, Inc., USA) with a DB-5 MS silica capillary column (i.d. 30 \times 0.25 mm,
165 0.25 μm film thickness). 1 μL sample was injected with splitless mode and high purity
166 helium (99.999%) was used as carrier gas at a stable flow of 1.0 mL/min. The GC
167 temperature was initiated at 100 $^\circ\text{C}$ (held for 1 min) and then to 300 $^\circ\text{C}$ at 5 $^\circ\text{C min}^{-1}$,
168 and kept at 300 $^\circ\text{C}$ for 10 min. The operation mode is electron ionization (EI) mode of
169 70 eV. The method detection limits (MDLs) for erythritol and PNA were 0.01 and 0.02
170 ng m^{-3} , respectively. The recoveries of erythritol, PNA, malic acid, PA and citramalic
171 acid were 67 \pm 2%, 73 \pm 1%, 75 \pm 1%, 88 \pm 7% and 82 \pm 8%, respectively. SOA tracers were
172 not detected in the field blank samples.

173 2.3 Observations in the air monitoring supersite

174 Water-soluble inorganic ions (WSII) in $\text{PM}_{2.5}$ (Cl^- , SO_4^{2-} , NO_3^- , Na^+ , K^+ , NH_4^+ ,
175 Mg^{2+} , and Ca^{2+}) and gas pollutants (HCl, HONO, HNO_3 , NH_3) were hourly measured

176 using a monitoring device for aerosols and gases in ambient Air (MARGA 2080;
177 Metrohm Applikon B.V.; Delft, Netherlands). Internal calibration was carried out using
178 LiBr standard solutions. The detection limit of Cl^- , SO_4^{2-} , NO_3^- , Na^+ , K^+ , NH_4^+ , Mg^{2+} ,
179 and Ca^{2+} were 0.01, 0.04, 0.05, 0.05, 0.09, 0.05, 0.06 and 0.09 $\mu\text{g m}^{-3}$, respectively.

180 Hourly mass concentrations of $\text{PM}_{2.5}$ and PM_{10} were measured by using a tapered
181 element oscillating microbalance (TEOM1405, Thermo Scientific Corp., MA, USA).
182 NO_2 , SO_2 , and O_3 were monitored using continuous gas analyzers (TEI 42i, 43i, and
183 49i, Thermo Scientific Corp., MA, USA). Ambient meteorological parameters
184 including relative humidity (RH), temperature (T), wind speed (WS), and wind
185 direction (WD) were obtained by an ultrasonic anemometer (150WX, Airmar, the
186 USA). Photolysis frequencies were determined using a photolysis spectrometer (PFS-
187 100, Focused Photonics Inc., Hangzhou, China), including the photolysis rate constants
188 $J(\text{O}^1\text{D})$, $J(\text{HCHO_M})$, $J(\text{HCHO_R})$, $J(\text{NO}_2)$, $J(\text{H}_2\text{O}_2)$, $J(\text{HONO})$, $J(\text{NO}_3_M)$ and
189 $J(\text{NO}_3_R)$, and the spectral band ranged from 270 to 790 nm. Boundary layer height
190 (BLH) based on ERA-5 reanalysis dataset was downloaded from the following link
191 <https://www.ecmwf.int/en/forecasts/datasets/reanalysis-datasets/era5>.

192 *2.4 Estimation of SOC using a tracer-based method*

193 The fraction of SOC formed by the oxidation of monoterpene, isoprene, β -
194 caryophyllene and toluene was estimated using a tracer-based method (Kleindienst et
195 al., 2007; Hong et al., 2019). It is defined as $[\text{SOC}] = \sum i[\text{tri}]/f_{\text{SOC}}$, where [SOC]
196 represents the mass concentration of SOC ($\mu\text{gC m}^{-3}$) and $\sum i[\text{tri}]$ means the sum of the
197 concentration of individual SOA tracer ($\mu\text{g m}^{-3}$). The carbon mass fractions (f_{SOC}) of
198 monoterpene, isoprene, β -caryophyllene and toluene were 0.231 ± 0.111 , 0.155 ± 0.039 ,
199 0.023 ± 0.005 and 0.008 ± 0.003 , respectively, based on smog-chamber experimental
200 data (Kleindienst et al., 2007).

201 *2.5 Aerosol acidity and OH calculation*

202 The forward mode of ISORROPIA II thermodynamic model was used to calculate
203 the aerosol acidity (pH) (Fountoukis and Nenes, 2007). ISORROPIA II can calculate

204 liquid water content (LWC), based on total SO_4^{2-} , NO_3^- (gas HNO_3 plus particle NO_3^-),
205 Cl^- , ammonia (gas NH_3 plus particle NH_4^+), non-volatile cations (Na^+ , K^+ , Ca^{2+} , Mg^{2+}),
206 and meteorological factors (RH and T) (Rumsey et al., 2014; Guo et al., 2016). The pH
207 value from ISORROPIA II was calculated using the following equation:

$$208 \quad \text{pH} = -\lg\left(\frac{1000 \times \text{H}^+}{\text{LWC}}\right)$$

209 where H^+ is the hydronium ion concentration loading for an air sample ($\mu\text{g}/\text{m}^3$).

210 The OH concentration ($[\text{OH}]$) was estimated using the NO_2 and HONO
211 concentrations and the photolysis rate constants (J) of NO_2 , O_3 , and HONO, according
212 to the following improved empirical formula (Wen et al., 2019).

$$213 \quad [\text{OH}] = 4.1 \times 10^9 \times \frac{J(\text{O}^1\text{D})^{0.83} \times J(\text{NO}_2)^{0.19} \times (140 \times \text{NO}_2 + 1) + \text{HONO} \times J(\text{HONO})}{0.41 \times \text{NO}_2^2 + 1.7 \times \text{NO}_2 + 1 + \text{NO} \times k_{\text{NO}+\text{OH}} + \text{HONO} \times k_{\text{HONO}+\text{OH}}}$$

214 2.6 Statistical analysis

215 Correlation analysis by SPSS 22.0 software (IBM, Armonk, NY, USA) was used
216 to study the relationship among SOA tracers, meteorological parameters and criteria air
217 pollutants. One-way analysis of variance (ANOVA) was adopted to examine the
218 variations of different factors.

219 2.7. Backward trajectory analysis

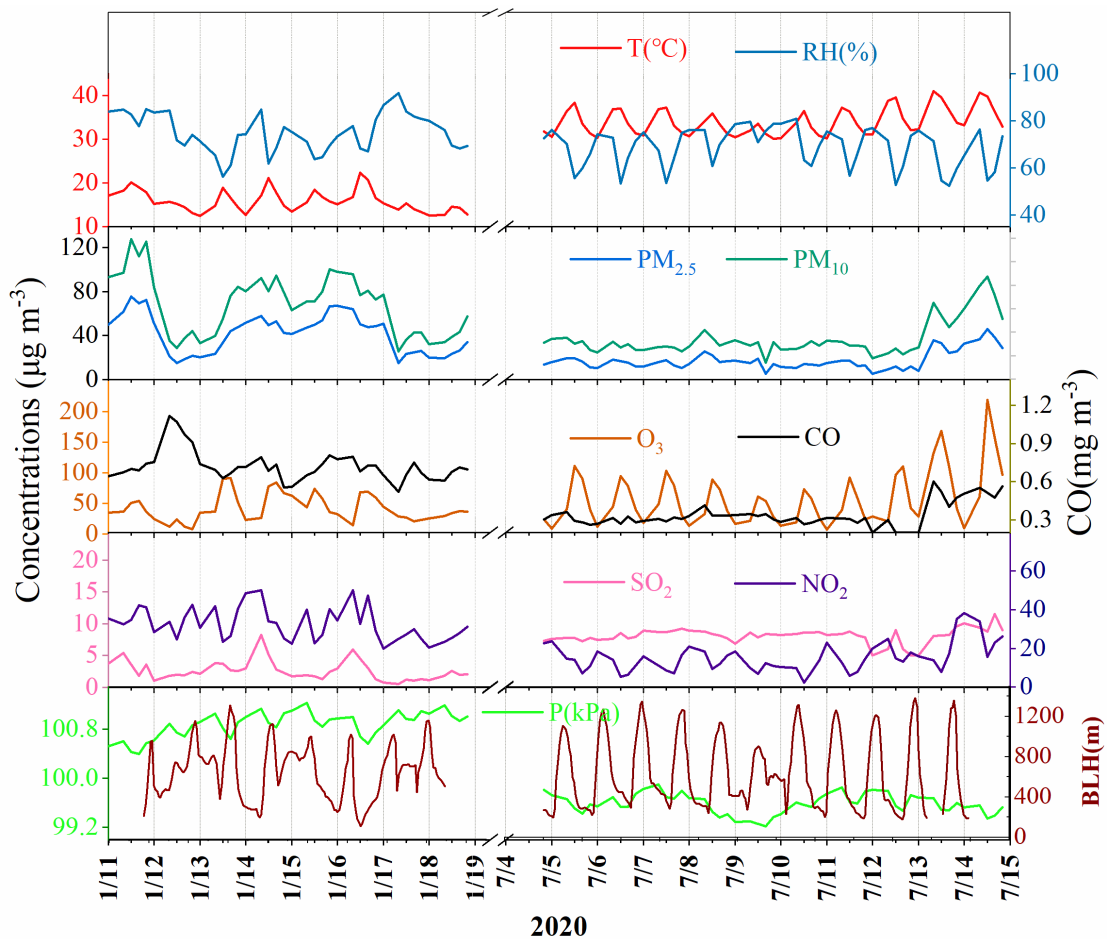
220 Hybrid Single-Particle Lagrangian Integrated Trajectory (HYSPLIT) was used to
221 analyze the impacts of air masses on Xiamen during different seasons. 72 h backward
222 trajectories were calculated every hour at a height of 500 m. The meteorological data
223 with a resolution of 1° longitude \times 1° latitude was obtained from the NCEP/GDAS.
224 Cluster analysis was adopted using the total spatial variance (TSV).

225 3 Results and discussion

226 3.1. Overview of air pollutants

227 The concentrations of criteria air pollutants, including SO_2 , CO, NO_2 , O_3 , $\text{PM}_{2.5}$
228 and PM_{10} , and meteorological parameters during wintertime and summertime were
229 shown in Fig.1. The concentrations of $\text{PM}_{2.5}$ in winter ranged from 14.9 to 75.3 $\mu\text{g m}^{-3}$
230 with an average of 42.1 $\mu\text{g m}^{-3}$, which was much higher than that (the average of 18.4

231 $\mu\text{g m}^{-3}$) in summer, ranging from 12.8 to 46.4 $\mu\text{g m}^{-3}$. The concentrations of CO, NO₂
 232 and PM₁₀ showed similar seasonal trends to the pattern of PM_{2.5}. In contrast, O₃ had the
 233 highest concentration in summer, which was attributed to the formation of
 234 photochemical reaction under strong UV radiation and the weak titration of nitrogen
 235 oxides. Meanwhile, the concentrations of SO₂ ($8.37\pm 0.79 \mu\text{g m}^{-3}$) in summer was also
 236 higher than that ($2.63\pm 1.95 \mu\text{g m}^{-3}$) in winter, mainly attributed to the influence of coal
 237 combustion and ship emissions. The monitoring site was located approximately 15 km
 238 away from Xiamen port area and a coal-fired power plant ($4 \times 300 \text{ kW}$) in the south.
 239 Southerly winds were prevailed in summer, which might cause the relative high
 240 concentration of SO₂ in the monitoring site.

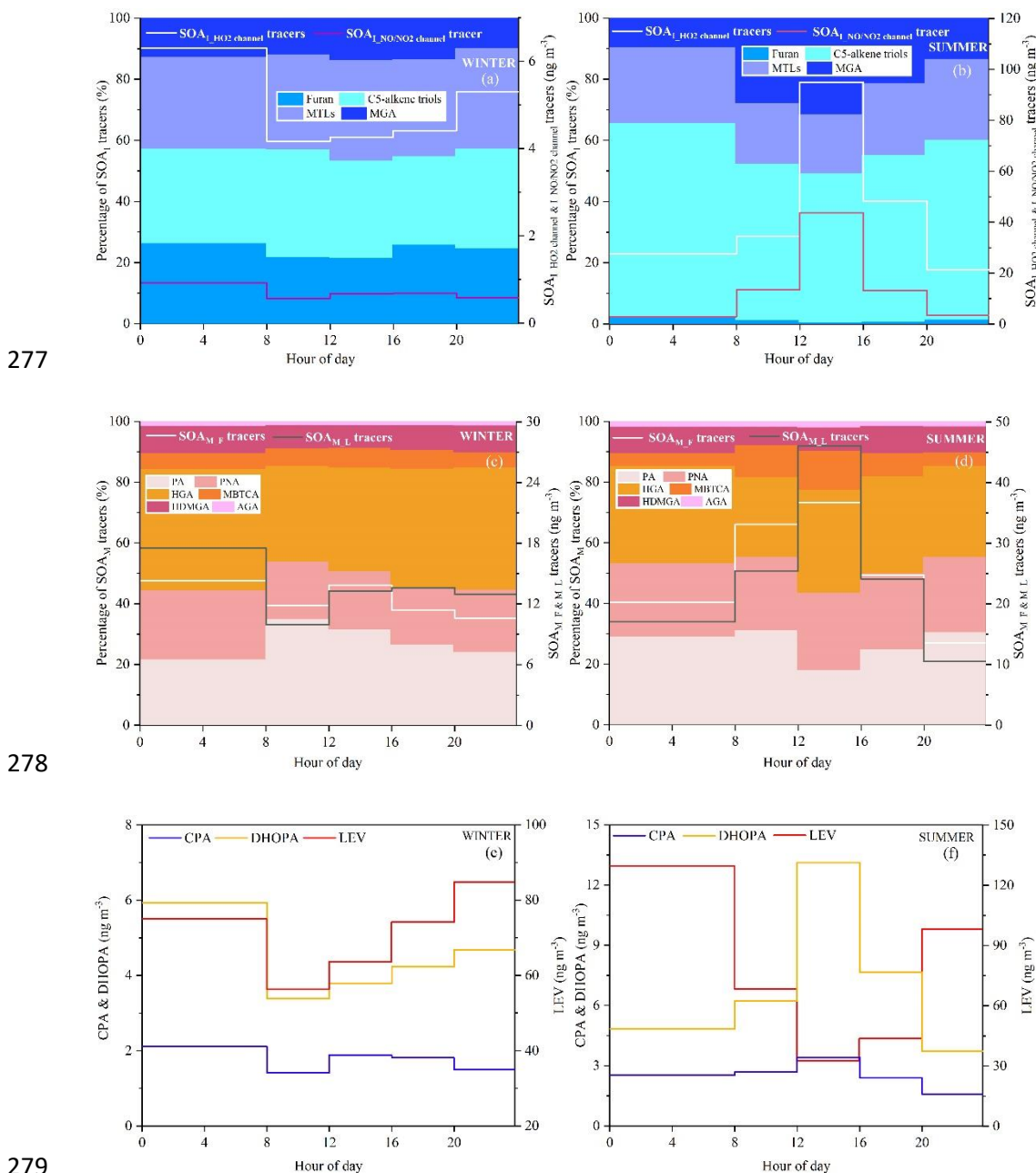


241
 242 **Figure 1. Time series of criteria air pollutants and meteorological parameters**
 243 **during the sampling period**

244 *3.2 Temporal variations of SOA tracers and estimated SOC*

245 Temporal variations of individual SOA tracer are shown in Fig.S1. The average
246 concentrations of total SOA tracers in winter and summer were 37.3 and 111.3 ng m⁻³,
247 respectively. The predominance of SOA_M (26.6 ng m⁻³), followed by ASOA (4.60 ng
248 m⁻³), SOA_I (4.35 ng m⁻³) and SOA_C (1.76 ng m⁻³) was observed in winter while SOA_I
249 (54.4 ng m⁻³) and SOA_M (47.8 ng m⁻³) in summer were the main contributors to total
250 SOA tracers, followed by ASOA (6.64 ng m⁻³) and SOA_C (2.45 ng m⁻³). In summer,
251 BSOA tracers showed much higher concentrations in the daytime (149.3 ng m⁻³) than
252 in the nighttime (60.1 ng m⁻³), while inverse results were observed in winter (30.4 ng
253 m⁻³ and 35.0 ng m⁻³ in the daytime and nighttime, respectively). As shown in Table S2,
254 in summer, SOA_I in the daytime ranged from 21.3 to 293.2 ng m⁻³ (average of
255 82.0±66.2 ng m⁻³) and the concentrations of SOA_I ranging from 6.81 to 110.1 ng m⁻³
256 (average of 26.8±24.6 ng m⁻³) were observed in the nighttime. However, in winter, the
257 concentrations of isoprene SOA tracers in the daytime ranging from 1.36 to 11.1 ng m⁻³
258 (average of 3.79±2.37ng m⁻³) were lower than those (average of 4.91±3.75 ng m⁻³) in
259 the nighttime. As shown in Fig. 2, diurnal variations of SOA_M, SOA_I, CPA and DHOPA
260 tracers in summer showed high levels in the afternoon (12:00–16:00 CST), due to the
261 impacts of beneficial photochemical oxidation conditions caused by high temperature
262 and strong UV radiation. The related SOA tracers were consisted with the emissions of
263 their precursors including biogenic and anthropogenic VOCs, similar to our previous
264 studies (Hong et al., 2019; Liu et al., 2020). However, the SOA tracers in winter showed
265 the lowest concentrations in the morning (8:00–12:00 CST), related with the favorable
266 dispersion conditions caused by the increasing planetary boundary layer height (BLH)
267 (Fig.1). Levoglucosan (LEV), a typical tracer of biomass burning, similar seasonal and
268 diurnal trend to other tracers was observed. However, LEV may not be as stable in the
269 atmosphere, especially under high relative humidity conditions (Hoffmann et al., 2010).
270 In this study, maybe, it's hard to reflect the real concentration of LEV. A correlation of
271 CPA with LEV was carried out (Fig.S2), just to discuss the impacts of biomass burning
272 on the distribution of CPA tracers through local or long-range transport. Totally, high
273 concentrations of BSOA tracers was found in the daytime and in summer, indicating

274 the effects of temperature on biogenic VOCs emissions and their photochemical
 275 oxidations. And the concentrations of BSOA tracers in winter increased in the nighttime,
 276 due to the changing of nocturnal boundary layer.



280 **Figure 2. Diurnal variation of individual SOA tracer during the wintertime (a, c,**
 281 **and e) and summertime (b, d, and f)**

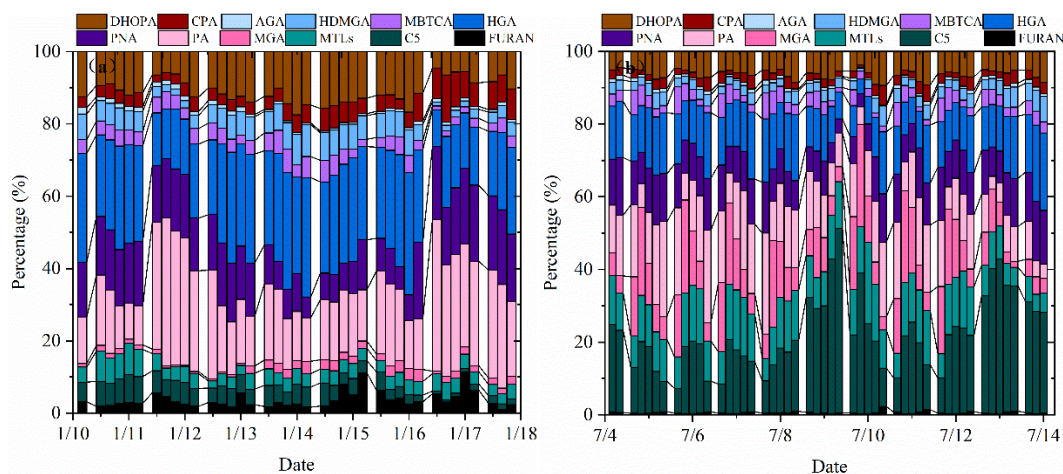
282 As shown in Fig.S2a, b, SOA tracers-based SOC in winter and summer was
 283 estimated. The concentrations of SOC in summer was higher than that in winter,

284 attributed to the increase of flourishing vegetation emissions and photochemical reactions
285 under high temperature and strong solar radiation conditions. For individual SOA tracer, the
286 concentrations of monoterpene-derived SOC was comparable to the toluene-derived
287 SOC, which were higher than isoprene-derived SOC and β -caryophyllene-derived SOC.
288 An obvious trend of diurnal variations of isoprene-derived SOC in summer was
289 observed, which was consistent with the diurnal pattern of isoprene concentration
290 (Fig.S3). However, no similar trend was found in winter, attributed to the influence of
291 low temperature on inhibiting the emissions of isoprene from various kinds of plants.
292 In addition, the toluene, monoterpene, isoprene and β -caryophyllene-derived SOC in
293 summer accounted for 40.0%, 39.2%, 15.7% and 5.1% of the total SOC, respectively
294 (Fig.S2c, d). However, in winter, the percentages of toluene, monoterpene, isoprene
295 and β -caryophyllene-derived SOC were 47.2%, 42.1%, 3.2% and 7.6%, respectively.
296 The percentages of isoprene-derived SOC estimated from different precursors varied
297 significantly among the seasons. High temperature enhanced the emissions of isoprene,
298 and strong solar radiation favored the formation of isoprene SOA tracers, contributing
299 to the highest isoprene-derived SOC percentage in summer (Ding et al., 2014). And the
300 highest percentages of toluene-derived SOC (47.2%) in winter were related with
301 anthropogenic emissions and adverse diffusion conditions.

302 *3.3 Atmospheric process indication of BSOA tracers*

303 As shown in Fig.3, percentages of different types of SOA tracers in winter and
304 summer were calculated. In summer, the monoterpene, isoprene, toluene and β -
305 caryophyllene SOA tracers accounted for 45.8%, 45.6%, 6.2% and 2.3% of the total
306 SOA tracers, respectively. However, in winter, the percentages of monoterpene,
307 isoprene, toluene and β -caryophyllene SOA tracers were 70.1%, 14.0%, 11.0% and
308 4.9%, respectively. The percentage of SOA_I tracers decreased sharply, due to the
309 impacts of temperature on isoprene emissions, which was consisted with our previous
310 findings (Hong et al., 2019). Meanwhile, the concentrations of SOA_M tracers were the
311 largest in both seasons, due to a large amount of monoterpene emissions from the
312 related plant species. Xiamen, an international garden city, located in coastal area of

313 southeastern China. Monoterpene, such as α/β -pinene, is mostly emitted by coniferous
 314 plant and most flowers and fruits, while isoprene originates from broad-leaved trees
 315 and deciduous plants (Ding et al., 2014; Shrivastava et al., 2017; Yang et al., 2021).



316

317 **Figure 3. Percentages of isoprene, monoterpene, β -caryophyllene and toluene**
 318 **SOA tracers in winter (a) and summer (b)**

319 The first (PA and PNA) and later generation (HGA, AGA, HDMGA and MBTCA)
 320 products were used to evaluate the aging degree of SOA_M (Ding et al., 2014; Hong et
 321 al., 2019). In this study, HGA (32.2%) was the major component of α/β -pinene tracers,
 322 followed by PA (30.5%), PNA (21.8%), HDMGA (7.3%), MBTCA (6.8%), and AGA
 323 (1.5%). The percentage of PA and PNA were much higher than those in mountainous
 324 background areas (PA: 9% and PNA: 3%)(Hong et al., 2019), suggesting the
 325 contribution of preliminary products to SOA in urban areas. As shown in Fig.3, the
 326 percentages of PA and PNA in winter (21.8% and 14.2%) were higher than those in
 327 summer (14.2% and 10.7%). Reacted with atmospheric oxidants including O₃ and OH,
 328 PA and PNA were transformed into MBTCA (Offenberg et al., 2007). This is the reason
 329 why the proportions of PA and PNA had a significant decreasing trend from winter to
 330 summer. The ratio of MBTCA/(PA+PNA) in summer and winter were 0.16±0.09 and
 331 0.12±0.07, respectively, which also proved the impacts of atmospheric oxidation
 332 capacity on the aging degree of SOA_M. In addition, the ratio of HGA/MBTCA could
 333 be used to distinguish the contribution of α -pinene or β -pinene to the SOA_M formation

334 (Jaoui et al., 2005; Ding et al., 2014). Low ratio of HGA/MBTCA (~1.0) showed that
335 α -pinene was the major precursor for SOA_M (Lewandowski et al., 2013). The ratio of
336 HGA/MBTCA with an average of 5.78 in Xiamen was high, suggesting the contribution
337 of β -pinene to SOA_M.

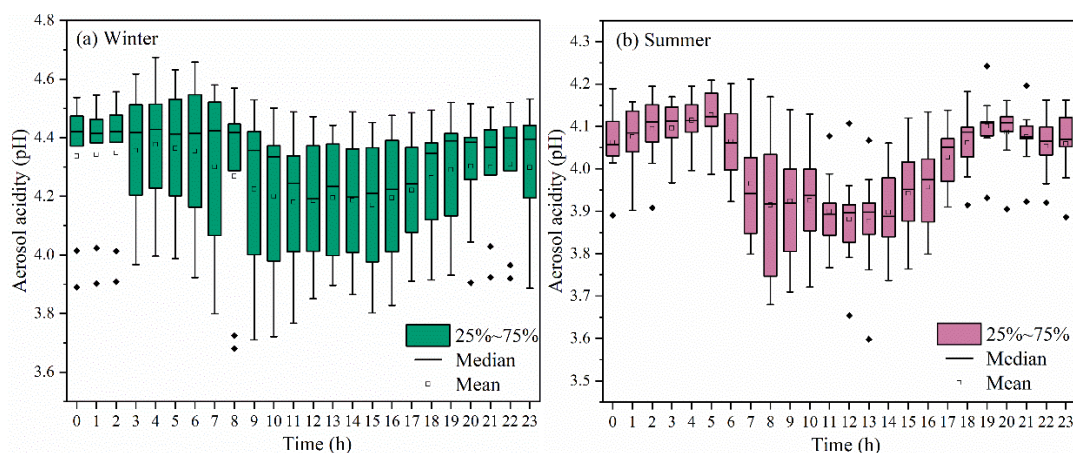
338 As shown in Fig.3, MTLs and C5 alkene triols were the main components of the
339 total SOA_I, with an average percentage of $68.0\pm 14.9\%$, indicating a low-NO_x
340 environment (Ding et al., 2014; Liu et al., 2020). In summer, the percentages of MTLs
341 and C5 alkene triols to the total SOA tracers in summer (21.8% and 14.2%) were
342 obviously higher than those in winter (4.2% and 4.3%). This was consisted with the
343 fact that the concentrations of NO₂ ($14.8\pm 7.46 \mu\text{g m}^{-3}$) in summer was significantly
344 lower than that ($32.7\pm 32.6 \mu\text{g m}^{-3}$) in winter. Previous studies found that MTLs and C5
345 alkene triols were formed by the OH and HO₂ radicals via the HO₂ channel under low-
346 NO_x conditions (Surratt et al., 2010). C5 alkene triols are mainly produced by acid
347 catalyzed reaction of Isoprene Epoxydiols (IEPOX) in the gas phase, while MTLs are
348 formed by ring opening products of IEPOX (Surratt et al., 2007; Surratt et al., 2010).
349 And the ozonolysis of isoprene was also an important pathway for MTLs in the
350 presence of acid sulfate aerosols (Riva et al., 2016).

351 CPA, the typical tracer of sesquiterpenes, is formed by the photooxidation of β -
352 caryophyllene (Jaoui et al., 2007). As shown in Fig.3, CPA in winter and summer
353 accounted for 5.0% and 2.3% of the total SOA tracers, respectively. This is because
354 that the percentage of SOA_I has significant increase in summer. And the concentrations
355 of CPA ($2.5\pm 2.0 \text{ ng m}^{-3}$) in summer were higher than that ($1.7\pm 0.8 \text{ ng m}^{-3}$) in winter,
356 probably attributed to the emissions of β -caryophyllene driven by temperature and solar
357 radiation. The CPA has a good correlation with DHOPA in summer (Fig.S4),
358 suggesting the influence of photochemical oxidation (Liu et al., 2020). However, the
359 CPA were not correlated with LEV in both seasons, reflecting the limited contribution
360 of biomass burning (Zhang et al., 2019c).

361 *3.4 Impacts of aerosol acidity on BSOA formation*

362 Aerosol acidity (pH) was an important factor on SOA formation (Surratt et al.,

363 2007; Offenberg et al., 2009; Zhang et al., 2019b; Zhang et al., 2019d). Time series of
 364 aerosol pH calculated by ISORROPIA II is shown in Fig.4. The PM_{2.5} in Xiamen was
 365 moderately acidic with daily pH range from 3.68 to 4.67. The highest aerosol pH was
 366 observed in winter, and the lowest pH in summer. This is with similar seasonal trend,
 367 closing to the Yangtze River Delta (YRD) region, but obviously lower levels than those
 368 in NCP cities of China (Zhou et al., 2021). In general, the aerosol pH in Chinese cities
 369 were higher than those in US and European.



370

371 **Figure 4. Diurnal variations of aerosol acidity (pH) during the wintertime (a)**
 372 **and summertime (b) period (The boxes with error bars represent the 10th, 25th,**
 373 **75th, and 90th percentiles)**

374 A declining trend pH during the daytime was observed (Fig. 4), which was related
 375 to the changes of chemical compositions and environmental conditions. The aerosol pH
 376 levels (~3 to 6) was related with a shift from sulfate- to nitrate-dominated aerosols (Guo
 377 et al., 2017). According to the multiphase buffer theory, the peak buffer pH (pKa*)
 378 regulated the aerosol pH, and temperature could obviously cause the variation of
 379 aerosol pH (Zheng et al., 2020). To further discuss the impacts of aerosol acidity on
 380 BSOA formation in coastal city, we analyzed the relationship between BSOA tracers
 381 and seed particles with different pH and liquid water content (LWC) (Fig. S5 and Table
 382 1).

Table 1 Correlations between individual BSOA tracer and environmental factors in winter and summer

Season	SOA tracer	pH	LWC	HONO	PM _{2.5}	Cl ⁻	NO ₃ ⁻	SO ₄ ²⁻	NH ₃	SO ₂	NO ₂	Ox	T	RH	UV
WINTER (n=39)	C5	.584**	.701**	.534**	.690**	.569**	.710**	.663**	.705**	0.308	.353*	0.203	.361*	0.140	0.200
	MTLS	.590**	.705**	.431*	.665**	.639**	.707**	.651**	.757**	0.185	0.229	0.098	.353*	0.295	-0.068
	MGA	.390*	.707**	0.261	.668**	0.081	.758**	.572**	0.284	0.172	0.123	.374*	.377*	-0.019	0.238
	PA	.432*	.403**	.463**	.407**	.481*	.416*	.488*	.440*	.446*	0.241	-0.193	.319*	-0.205	0.145
	PNA	.489**	.579**	0.311	.459**	.516**	.573**	.533**	.543**	0.08	0.071	-0.101	0.121	.337*	-0.122
	HGA	.443*	.829**	.352*	.834**	.600**	.847**	.754**	.641**	0.275	0.299	.451**	.451**	0.043	0.210
	MBTCA	.433*	.678**	.447**	.670**	.435*	.733**	.589**	.710**	.327*	0.253	.492**	.552**	-0.158	0.317
	HDMGA	.421*	.876**	.401*	.867**	.631**	.884**	.813**	.643**	.335*	.321*	.526**	.485**	-0.049	0.327
	AGA	.570**	.575**	.370*	.488**	.577**	.566**	.544**	.731**	0.126	0.181	0.019	0.279	0.298	-0.122
	CPA	0.212	.462**	-0.068	.452**	.483**	.437*	.419*	.419*	-0.15	-0.170	0.016	0.079	0.200	-0.144
SUMMER (n=50)	C5	-.495**	.425**	0.160	.622**	-.340*	0.268	.625**	.436**	0.254	0.025	.649**	.573**	-.529**	0.247
	MTLS	-.551**	0.131	0.055	0.272	-.439**	0.131	.428**	.304*	0.089	-0.278	.550**	.610**	-.594**	0.263
	MGA	-.540**	0.029	0.116	0.132	-.403**	0.066	.472**	0.270	0.096	-0.410**	.443**	.633**	-.668**	.382*
	PA	-.633**	.483**	.601**	.461**	-0.135	.541**	.502**	.405*	0.037	0.238	.456**	.626**	-.558**	.400*
	PNA	-.664**	.616**	.387**	.812**	-.389**	.450**	.784**	.503**	0.269	.294*	.769**	.718**	-.631**	.404*
	HGA	-.607**	.612**	.299*	.836**	-.384**	.447**	.770**	.539**	.316*	0.272	.808**	.670**	-.599**	0.322
	MBTCA	-.752**	.415**	0.237	.577**	-.382**	.359*	.636**	.501**	0.201	-0.052	.712**	.852**	-.816**	.588**
	HDMGA	-.525**	.618**	.299*	.833**	-.342*	.408**	.768**	.488**	.358*	.365**	.746**	.574**	-.500**	0.240
	AGA	-.684**	.592**	.447**	.766**	-.334*	.479**	.735**	.435**	0.244	0.271	.694**	.720**	-.634**	.477**
	CPA	-.552**	.625**	.441**	.780**	-.280*	.453**	.763**	.307*	.299*	.503**	.611**	.529**	-.458**	0.305

384 **Correlation coefficients with an asterisk indicate statistically significant relationships at $\alpha = 0.05$, and two asterisks mean significant at $\alpha = 0.01$.

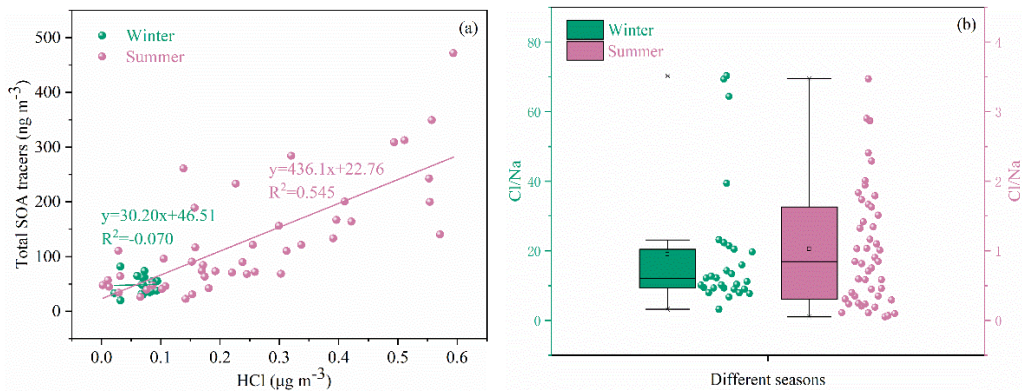
387 In Table 1, the BSOA tracers was linearly correlated with aerosol acidity (pH) and
388 SO_4^{2-} . In summer, BSOA tracers in the particle phase were found to increase with
389 increasing acidity, which was attributed to the presence of acid catalyzed aerosols. For
390 example, isoprene SOA tracers is mainly formed through acid-catalyzed reactive uptake
391 of isoprene-derived epoxydiols (IEPOX) onto sulfate aerosol particles. In our previous
392 studies, we have reported that high concentration of MTLs was related with sulfate,
393 which could significantly promote the formation of isoprene-SOA tracers (Liu et al.,
394 2020). Other studies also found that sulfate could increase the BSOA production by
395 promoting acid-catalyzed ring-opening reactions (Xu et al., 2015). In contrast, positive
396 correlations between BSOA tracers and aerosol pH in winter were observed, indicating
397 that the formation of BSOA was predominantly enhanced by other factors, except for
398 the aerosol acidity. The aerosol pH in winter was higher than those in summer, probably
399 due to the influence of nitrate-dominated aerosols. Also, the aged aerosols through long-
400 range transport might result in the increase of BSOA tracers and aerosol pH.

401 In addition, positive correlation between BSOA tracers and LWC was observed
402 (Table 1), probably attributed to the effects of the LWC on determining the peak buffer
403 pH (pK_a^*). Zheng et al. (2020) reported that the buffering effect of ammonia suppresses
404 the contribution of different chemical compositions in aerosol particles, making LWC
405 the primary determinant of aerosol pH. Other studies have demonstrated that the uptake
406 coefficient of first-generation oxidation products, especially for carbonyl compounds,
407 might depend on RH (Luo et al., 2019). Meanwhile, high LWC could reduce the aerosol
408 particle viscosity, which was benefit to the generation of the reactive intermediate such
409 as IEPOX, or other oxidation products of VOC into aqueous-phase of aerosol particles,
410 thereby promoting the formation of BSOA (Zhang et al., 2019b; Zhang et al., 2019d).

411 *3.5 Impacts of chlorine on BSOA formation*

412 Halogen radicals (Cl, Br and I) originated from sea salt aerosol (SSA) have an
413 important role in tropospheric oxidants chemistry (Wang et al., 2021c). In this study,
414 chlorine depletion was frequently observed in summer (Fig.5b), indicating that HCl can
415 be formed through acid displacement of sea salt aerosol Cl^- by H_2SO_4 and HNO_3
416 produced from anthropogenic emissions of SO_2 and NO_x . Moreover, concentrations of
417 the total SOA tracers were positively correlated with HCl (Fig.5a), suggesting the
418 enhancement of SOA precursors transformation. Previous studies have found that Cl-
419 initiated VOC oxidations could contribute to the formation of SOA (Wang and Ruiz,

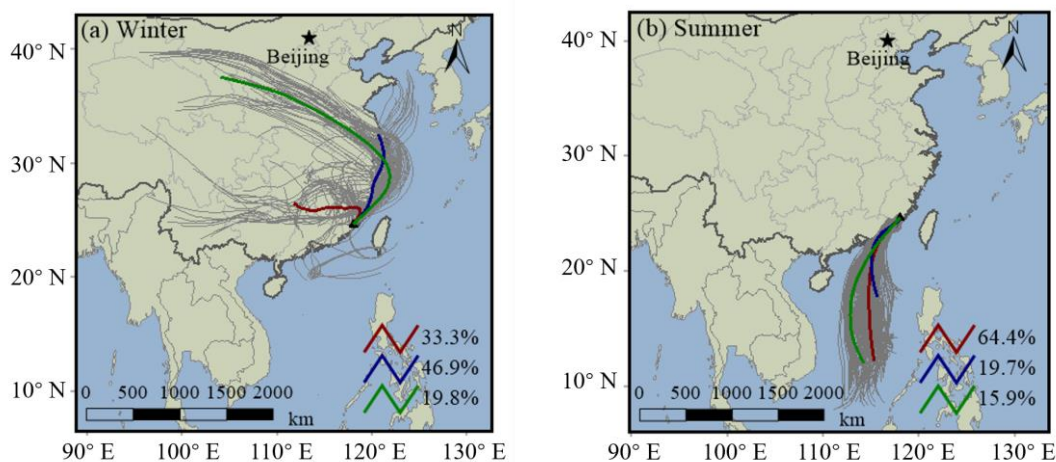
420 2017; Dhulipala et al., 2019).



421

422 **Figure 5. Correlations of total SOA tracers and HCl (a) and chlorine depletion**
 423 **(b) in different seasons**

424 Under ammonia-rich conditions, HCl partitioned into the aqueous particulate
 425 phase mostly took place, and chlorine ions could affect aqueous oxidation of secondary
 426 organic compounds (Xu et al., 2021). As shown in Table 1, most of SOA tracers in
 427 winter were correlated with the concentrations of chlorine ions in PM_{2.5}, while inverse
 428 results were observed in summer. In winter, the dominant wind direction is northeast
 429 (Fig.6), and chlorine mainly come from continental polluted air mass, such as industrial
 430 and combustion emissions. So, anthropogenic pollutants through long-range transport
 431 might cause the enhancement of SOA tracer concentrations at the monitoring site.
 432 However, in summer, negative correlations of BSOA tracers and chlorine ions in PM_{2.5}
 433 was found, probably due to the influence of chlorine depletion. As shown in Fig. 6, the
 434 dominant wind direction is southerly, and chlorine mainly originated from the spray of
 435 sea salt.



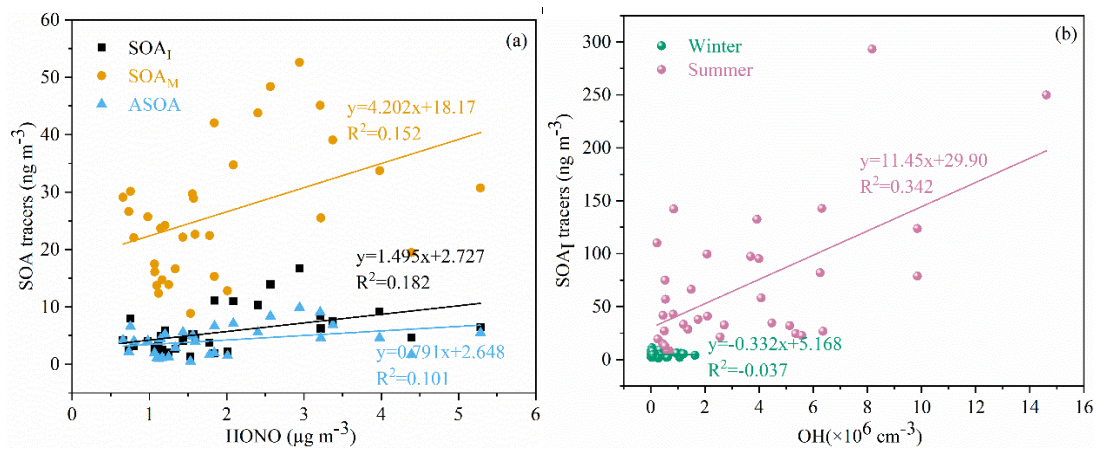
436

437 **Figure 6. Backward trajectories analyses during the winter (a) and summertime**
 438 **(b)**

439 *3.6. Enhanced formation of BSOA by anthropogenic emissions*

440 Recent studies had indicated that anthropogenic emissions might affect SOA
 441 formation through multiple chemical processes, based on laboratory studies and field
 442 observations (Kari et al., 2019; Shrivastava et al., 2019; Zhang et al., 2019c; Cheng et
 443 al., 2021; Xu et al., 2021). In this study, we conducted the correlation analysis of
 444 individual SOA tracers and Ox (=O₃+NO₂), HONO, OH, SO₂, NH₃, PM_{2.5}, sulfate,
 445 nitrate, as well as meteorological parameters (including T, RH and UV) (Table 1).

446 Most of SOA tracers have a significant positive correlation with NH₃, suggesting
 447 an enhancement effect on the formation of SOA (Table 1). NH₃ could affect the SOA
 448 yields through both gas-phase and heterogeneous reactions (Na et al., 2007; Ma et al.,
 449 2018; Hao et al., 2020). Gas-phase reaction between NH₃ and organic acids (such as
 450 PA and PNA) produced ammonium salts in the particle phase, which contributed to the
 451 increased SOA formation. However, not all gas-phase organic acids (e.g., MGA and
 452 pyruvic acid) could demonstrate gas-to-particle conversion (Na et al., 2007). When
 453 SOA formation had ceased, the addition of excessive NH₃ would result in the rapid
 454 decomposition of the main SOA species, due to the nucleophilic attack of NH₃ (Ma et
 455 al., 2018).



456

457 **Figure 7. Relationships of SOA tracers and HONO (a) and its estimated OH (b)**

458 As an indicator of atmospheric oxidation capacity, the tropospheric odd oxygen
 459 Ox (O₃+NO₂) was calculated. As shown in Table 1, the majority of SOA tracers in
 460 summer showed significant positive correlations with Ox (R>0.5, P<0.001). However,
 461 in winter, a part of SOA_M tracers (e.g. HGA, MBTCA and HDMGA) were found to be

462 significantly correlated with Ox. In addition, HONO and OH radicals, another critical
463 indicator of atmospheric oxidation capacity, was also discussed. In this study, the
464 concentration of OH radicals calculated from HONO in summer was higher than those
465 in winter. In summer, the SOA_I tracers was correlated with OH radicals (Fig.7b),
466 consisted with previous findings that OH radicals could promote the formation of SOA
467 (Sarrafzadeh et al., 2016; Liu et al., 2019; Song et al., 2019; Zhang et al., 2019a). Due
468 to its photolysis to produce OH radicals during the daytime, HONO could facilitate
469 SOA formation. In winter, the concentrations of SOA_I, SOA_M and ASOA tracers were
470 correlated with HONO (Fig.7a). These results indicated high concentrations of HONO
471 and sufficient ultraviolet radiation could enhance the photochemical reactions of VOCs.
472 Which was consisted with our previous results on the formation of peroxyacetyl nitrate
473 (PAN) (Hu et al., 2020). As for T and UV, it exhibited significantly positive correlations
474 with the related SOA tracers, especially in summer. These results suggested that SOA
475 tracers were produced from the photo-oxidation of VOC precursors (Cheng et al., 2021).

476 In addition, the SOA tracers were significantly positive correlated with PM_{2.5} and
477 its components including NO₃⁻ and SO₄²⁻. In coastal cities of southeastern China, with
478 the development of rapid urbanization, air pollution caused by motor vehicles and
479 industrial emissions is becoming more frequent in winter (Wu et al., 2020). The Xiamen
480 port is one of the top 10 ports in China, resulting the impacts of ship emissions and port
481 activities on ambient air quality (Xu et al., 2018), and the numbers of motor vehicles
482 increased sharply in recent years. We also found that the 90th percentile of maximum
483 daily average 8h (MDA8) O₃ concentrations in Xiamen was significantly increased
484 from 2015 to 2020 (Fig. S6). During the past several years, the elevated secondary
485 inorganic components, including NO₃⁻, SO₄²⁻ and NH₄⁺, accounted for 40-50% of the
486 total PM_{2.5}, and OM ranged from 30% to 40% (Wu et al., 2019; Hong et al., 2021).
487 These results also implied the effects of anthropogenic emissions and enhanced
488 atmospheric oxidation capacity on secondary formation of aerosol particles under
489 atmospheric stagnant conditions.

490 **Conclusions**

491 Pollution characteristics and source identification of BSOA tracers during the
492 summer and winter in coastal areas of southeastern China were investigated. The
493 average concentration of total BSOA tracers in summer was higher than that in winter,

494 with the predominance of SOA_M, followed by SOA_I and SOA_C. The BSOA tracers in
495 summer were predominantly produced by the influence of photochemical oxidation
496 under relatively clean conditions. However, in winter, the formation of BSOA tracers
497 were attributed to the impacts of anthropogenic emissions and atmospheric stagnant
498 conditions. In addition, the results also indicated that acid-catalyzed reactive uptake
499 onto sulfate aerosol particles enhanced the formation of BSOA in both seasons. We
500 further found that Cl-initiated VOC oxidations has potentially accelerated the
501 transformation of BSOA precursors through sea salt aerosol originated from the ocean
502 in summer and anthropogenic emissions in winter. This study demonstrated that the
503 combined effects of anthropogenic pollutants and atmospheric oxidation capacity on
504 the formation of BSOA in coastal area.

505

506 **Data Availability.** The data set related to this work can be accessed via
507 <https://doi.org/10.5281/zenodo.6376025> (Hong, 2022). The details are also available
508 upon request from the corresponding author (ywhong@iue.ac.cn).

509

510 **Authorship Contribution Statement.** Youwei Hong and Xinbei Xu contributed equally
511 to this work. Youwei Hong designed and wrote the manuscript. Xinbei Xu collected the
512 data, contributed to the data analysis. Dan Liao, Taotao Liu, Xiaoting Ji and Ke Xu
513 performed modeling analyses and data analysis. Jinsheng Chen supported funding of
514 observation and research. Chunyang Liao, Ting Wang and Chunshui Lin contributed to
515 revise the manuscript.

516

517 **Competing interests.** The authors declare that they have no conflict of interest.

518

519 **Acknowledgement.** The authors gratefully acknowledge Yanting Chen, Han Zhang and
520 Xu Liao (Institute of Urban Environment, Chinese Academy of Sciences) for the
521 guidance and assistance during sample pretreatment, and Lingling Xu and Mengren Li
522 (Institute of Urban Environment, Chinese Academy of Sciences) for the discussion of
523 this paper. This study was supported by Fujian Key Laboratory of Atmospheric Ozone
524 Pollution Prevention and Xiamen Atmospheric Environment Observation and Research
525 Station of Fujian Province (Institute of Urban Environment, Chinese Academy of
526 Sciences).

527

528 **Financial support.** This research was financially supported by the foreign cooperation
529 project of Fujian Province (2020I0038), the Xiamen Youth Innovation Fund Project
530 (3502Z20206094), the Cultivating Project of Strategic Priority Research Program of
531 Chinese Academy of Sciences (XDPB1903), the National Key Research and
532 Development Program (2016YFC0112200), State Key Laboratory of Environmental
533 Chemistry and Ecotoxicology, Research Center for Eco-Environmental Sciences, CAS
534 (KF2020-06), the FJIRSM&IUE Joint Research Fund (RHZX-2019-006) and center for
535 Excellence in Regional Atmospheric Environment project (E0L1B20201).

536

537 Reference

- 538 Charan, S. M., Huang, Y., and Seinfeld, J. H.: Computational Simulation of Secondary
539 Organic Aerosol Formation in Laboratory Chambers, *Chem. Rev.*, 119, 11912-11944,
540 10.1021/acs.chemrev.9b00358, 2019.
- 541 Cheng, Y., Ma, Y., and Hu, D.: Tracer-based source apportioning of atmospheric organic
542 carbon and the influence of anthropogenic emissions on secondary organic aerosol
543 formation in Hong Kong, *Atmos. Chem. Phys.*, 21, 10589-10608, 10.5194/acp-21-
544 10589-2021, 2021.
- 545 Dhulipala, S. V., Bhandari, S., and Hildebrandt Ruiz, L.: Formation of oxidized organic
546 compounds from Cl-initiated oxidation of toluene, *Atmospheric Environment*, 199, 265-
547 273, 10.1016/j.atmosenv.2018.11.002, 2019.
- 548 Ding, X., He, Q.-F., Shen, R.-Q., Yu, Q.-Q., and Wang, X.-M.: Spatial distributions of
549 secondary organic aerosols from isoprene, monoterpenes, beta-caryophyllene, and
550 aromatics over China during summer, *Journal of Geophysical Research-Atmospheres*,
551 119, 11877-11891, 10.1002/2014jd021748, 2014.
- 552 Fountoukis, C., and Nenes, A.: ISORROPIA II: a computationally efficient
553 thermodynamic equilibrium model for $K^+ - Ca^{2+} - Mg^{2+} - NH_4^+ - Na^+ - SO_4^{2-} -$
554 $NO_3^- - Cl^- - H_2O$ aerosols, *Atmos. Chem. Phys.*, 7, 4639-4659, 10.5194/acp-7-
555 4639-2007, 2007.
- 556 Fu, P., Kawamura, K., Chen, J., and Barrie, L. A.: Isoprene, Monoterpene, and Sesquiterpene
557 Oxidation Products in the High Arctic Aerosols during Late Winter to Early Summer,
558 *Environmental Science & Technology*, 43, 4022-4028, 10.1021/es803669a, 2009.
- 559 Guo, H., Sullivan, A. P., Campuzano-Jost, P., Schroder, J. C., Lopez-Hilfiker, F. D.,
560 Dibb, J. E., Jimenez, J. L., Thornton, J. A., Brown, S. S., Nenes, A., and Weber,
561 R. J.: Fine particle pH and the partitioning of nitric acid during winter in the
562 northeastern United States, *Journal of Geophysical Research: Atmospheres*, 121,
563 10,355-310,376, <https://doi.org/10.1002/2016JD025311>, 2016.
- 564 Guo, H., Weber, R. J., and Nenes, A.: High levels of ammonia do not raise fine particle pH
565 sufficiently to yield nitrogen oxide-dominated sulfate production, *Scientific Reports*, 7,
566 12109, 10.1038/s41598-017-11704-0, 2017.
- 567 Hallquist, M., Wenger, J. C., Baltensperger, U., Rudich, Y., Simpson, D., Claeys, M.,
568 Dommen, J., Donahue, N. M., George, C., Goldstein, A. H., Hamilton, J. F., Herrmann,
569 H., Hoffmann, T., Iinuma, Y., Jang, M., Jenkin, M. E., Jimenez, J. L., Kiendler-Scharr,
570 A., Maenhaut, W., McFiggans, G., Mentel, T. F., Monod, A., Prevot, A. S. H., Seinfeld,
571 J. H., Surratt, J. D., Szmigielski, R., and Wildt, J.: The formation, properties and impact

572 of secondary organic aerosol: current and emerging issues, *Atmospheric Chemistry and*
573 *Physics*, 9, 5155-5236, 10.5194/acp-9-5155-2009, 2009.

574 Hao, L., Kari, E., Leskinen, A., Worsnop, D. R., and Virtanen, A.: Direct contribution of
575 ammonia to α -pinene secondary organic aerosol formation, *Atmos. Chem. Phys.*, 20,
576 14393-14405, 10.5194/acp-20-14393-2020, 2020.

577 Hoffmann, D., Tilgner, A., Iinuma, Y., and Herrmann, H.: Atmospheric Stability of
578 Levoglucosan: A Detailed Laboratory and Modeling Study, *Environmental Science &*
579 *Technology*, 44, 694-699, 10.1021/es902476f, 2010.

580 Hong, Y., Xu, X., Liao, D., Zheng, R., Ji, X., Chen, Y., Xu, L., Li, M., Wang, H., Xiao, H.,
581 Choi, S.-D., and Chen, J.: Source apportionment of PM_{2.5} and sulfate formation during
582 the COVID-19 lockdown in a coastal city of southeast China, *Environmental Pollution*,
583 286, 117577, <https://doi.org/10.1016/j.envpol.2021.117577>, 2021.

584 Hong, youwei. (2022). Dataset for ACP by Hong et al., 2022 [Data set]. Zenodo.
585 <https://doi.org/10.5281/zenodo.6376025>

586 Hong, Z., Zhang, H., Zhang, Y., Xu, L., Liu, T., Xiao, H., Hong, Y., Chen, J., Li, M., Deng,
587 J., Wu, X., Hu, B., and Chen, X.: Secondary organic aerosol of PM_{2.5} in a mountainous
588 forest area in southeastern China: Molecular compositions and tracers implication,
589 *Science of the Total Environment*, 653, 496-503, 10.1016/j.scitotenv.2018.10.370, 2019.

590 Hoyle, C. R., Boy, M., Donahue, N. M., Fry, J. L., Glasius, M., Guenther, A., Hallar, A. G.,
591 Hartz, K. H., Petters, M. D., Petaja, T., Rosenoern, T., and Sullivan, A. P.: A review of
592 the anthropogenic influence on biogenic secondary organic aerosol, *Atmospheric*
593 *Chemistry and Physics*, 11, 321-343, 10.5194/acp-11-321-2011, 2011.

594 Hu, B., Liu, T., Hong, Y., Xu, L., Li, M., Wu, X., Wang, H., Chen, J., and Chen, J.:
595 Characteristics of peroxyacetyl nitrate (PAN) in a coastal city of southeastern China:
596 Photochemical mechanism and pollution process, *Science of the Total Environment*,
597 719, 10.1016/j.scitotenv.2020.137493, 2020.

598 Hu, W., Palm, B. B., Day, D. A., Campuzano-Jost, P., Krechmer, J. E., Peng, Z., de Sa, S. S.,
599 Martin, S. T., Alexander, M. L., Baumann, K., Hacker, L., Kiendler-Scharr, A., Koss, A.
600 R., de Gouw, J. A., Goldstein, A. H., Seco, R., Sjostedt, S. J., Park, J.-H., Guenther, A.
601 B., Kim, S., Canonaco, F., Prevot, A. S. H., Brune, W. H., and Jimenez, J. L.: Volatility
602 and lifetime against OH heterogeneous reaction of ambient isoprene-epoxydiols-derived
603 secondary organic aerosol (IEPOX-SOA), *Atmospheric Chemistry and Physics*, 16,
604 11563-11580, 10.5194/acp-16-11563-2016, 2016.

605 Jaoui, M., Kleindienst, T. E., Lewandowski, M., Offenber, J. H., and Edney, E. O.:
606 Identification and quantification of aerosol polar oxygenated compounds bearing
607 carboxylic or hydroxyl groups. 2. Organic tracer compounds from monoterpenes,
608 *Environmental Science & Technology*, 39, 5661-5673, 10.1021/es048111b, 2005.

609 Jaoui, M., Lewandowski, M., Kleindienst, T. E., Offenber, J. H., and Edney, E. O.: β -
610 caryophyllinic acid: An atmospheric tracer for β -caryophyllene secondary organic
611 aerosol, *Geophysical Research Letters*, 34, 10.1029/2006gl028827, 2007.

612 Kari, E., Hao, L. Q., Ylisirnio, A., Buchholz, A., Leskinen, A., Yli-Pirila, P., Nuutinen, I.,
613 Kuusalo, K., Jokiniemi, J., Faiola, C. L., Schobesberger, S., and Virtanen, A.: Potential
614 dual effect of anthropogenic emissions on the formation of biogenic secondary organic
615 aerosol (BSOA), *Atmospheric Chemistry and Physics*, 19, 15651-15671, 10.5194/acp-
616 19-15651-2019, 2019.

617 Kleindienst, T. E., Jaoui, M., Lewandowski, M., Offenber, J. H., Lewis, C. W., Bhave, P. V.,
618 and Edney, E. O.: Estimates of the contributions of biogenic and anthropogenic
619 hydrocarbons to secondary organic aerosol at a southeastern US location, *Atmospheric*
620 *Environment*, 41, 8288-8300, 10.1016/j.atmosenv.2007.06.045, 2007.

621 Lewandowski, M., Piletic, I. R., Kleindienst, T. E., Offenber, J. H., Beaver, M. R., Jaoui, M.,
622 Docherty, K. S., and Edney, E. O.: Secondary organic aerosol characterisation at field
623 sites across the United States during the spring-summer period, *International Journal of*

624 Environmental Analytical Chemistry, 93, 1084-1103, 10.1080/03067319.2013.803545,
625 2013.

626 Liu, S., Tsona, N. T., Zhang, Q., Jia, L., Xu, Y., and Du, L.: Influence of relative humidity on
627 cyclohexene SOA formation from OH photooxidation, *Chemosphere*, 231, 478-486,
628 10.1016/j.chemosphere.2019.05.131, 2019.

629 Liu, S., Huang, D., Wang, Y., Zhang, S., Wu, C., Du, W., and Wang, G.: Synergetic effect of
630 NH₃ and NO_x on the production and optical absorption of secondary organic aerosol
631 formation from toluene photooxidation, *Atmos. Chem. Phys. Discuss.*, 2021, 1-38,
632 10.5194/acp-2021-560, 2021.

633 Liu, T., Hu, B., Xu, X., Hong, Y., Zhang, Y., Wu, X., Xu, L., Li, M., Chen, Y., Chen, X., and
634 Chen, J.: Characteristics of PM_{2.5}-bound secondary organic aerosol tracers in a coastal
635 city in Southeastern China: Seasonal patterns and pollution identification, *Atmospheric
636 Environment*, 237, 10.1016/j.atmosenv.2020.117710, 2020.

637 Lopez-Hilfiker, F. D., Mohr, C., D'Ambro, E. L., Lutz, A., Riedel, T. P., Gaston, C. J., Iyer,
638 S., Zhang, Z., Gold, A., Surratt, J. D., Lee, B. H., Kurten, T., Hu, W. W., Jimenez, J.,
639 Hallquist, M., and Thornton, J. A.: Molecular Composition and Volatility of Organic
640 Aerosol in the Southeastern US: Implications for IEPDX Derived SOA, *Environmental
641 Science & Technology*, 50, 2200-2209, 10.1021/acs.est.5b04769, 2016.

642 Lowes, S., Jersey, J., Shoup, R., Garofolo, F., Savoie, N., Mortz, E., Needham, S., Caturla, M.
643 C., Steffen, R., Sheldon, C., Hayes, R., Samuels, T., Di Donato, L., Kamerud, J.,
644 Michael, S., Lin, Z. P., Hillier, J., Moussallie, M., Teixeira, L. D., Rocci, M., Buonarati,
645 M., Truog, J., Hussain, S., Lundberg, R., Breau, A., Zhang, T. Y., Jonker, J., Berger, N.,
646 Gagnon-Carignan, S., Nehls, C., Nicholson, R., Hilhorst, M., Karnik, S., de Boer, T.,
647 Houghton, R., Smith, K., Cojocar, L., Allen, M., Harter, T., Fatmi, S., Sayyarpour, F.,
648 Vija, J., Malone, M., and Heller, D.: Recommendations on: internal standard criteria,
649 stability, incurred sample reanalysis and recent 483s by the Global CRO Council for
650 Bioanalysis, *Bioanalysis*, 3, 1323-1332, 10.4155/Bio.11.135, 2011.

651 Luo, H., Jia, L., Wan, Q., An, T., and Wang, Y.: Role of liquid water in the formation of O-3
652 and SOA particles from 1,2,3-trimethylbenzene, *Atmospheric Environment*, 217,
653 10.1016/j.atmosenv.2019.116955, 2019.

654 Lv, S., Wang, F., Wu, C., Chen, Y., Liu, S., Zhang, S., Li, D., Du, W., Zhang, F., Wang, H.,
655 Huang, C., Fu, Q., Duan, Y., and Wang, G.: Gas-to-Aerosol Phase Partitioning of
656 Atmospheric Water-Soluble Organic Compounds at a Rural Site in China: An Enhancing
657 Effect of NH₃ on SOA Formation, *Environmental Science & Technology*,
658 10.1021/acs.est.1c06855, 2022.

659 Ma, Q., Lin, X. X., Yang, C. G., Long, B., Gai, Y. B., and Zhang, W. J.: The influences of
660 ammonia on aerosol formation in the ozonolysis of styrene: roles of Criegee intermediate
661 reactions, *Roy Soc Open Sci*, 5, ARTN 17217110.1098/rsos.172171, 2018.

662 Mahilang, M., Deb, M. K., and Pervez, S.: Biogenic secondary organic aerosols: A review on
663 formation mechanism, analytical challenges and environmental impacts, *Chemosphere*,
664 262, 10.1016/j.chemosphere.2020.127771, 2021.

665 McFiggans, G., Mentel, T. F., Wildt, J., Pullinen, I., Kang, S., Kleist, E., Schmitt, S.,
666 Springer, M., Tillmann, R., Wu, C., Zhao, D. F., Hallquist, M., Faxon, C., Le Breton, M.,
667 Hallquist, A. M., Simpson, D., Bergstrom, R., Jenkin, M. E., Ehn, M., Thornton, J. A.,
668 Alfarra, M. R., Bannan, T. J., Percival, C. J., Priestley, M., Topping, D., and Kiendler-
669 Scharr, A.: Secondary organic aerosol reduced by mixture of atmospheric vapours,
670 *Nature*, 565, 587-593, 10.1038/s41586-018-0871-y, 2019.

671 Na, K., Song, C., Switzer, C., and Cocker, D. R.: Effect of Ammonia on Secondary Organic
672 Aerosol Formation from α -Pinene Ozonolysis in Dry and Humid Conditions,
673 *Environmental Science & Technology*, 41, 6096-6102, 10.1021/es061956y, 2007.

674 Newland, M. J., Bryant, D. J., Dunmore, R. E., Bannan, T. J., Acton, W. J. F., Langford, B.,
675 Hopkins, J. R., Squires, F. A., Dixon, W., Drysdale, W. S., Ivatt, P. D., Evans, M. J.,
676 Edwards, P. M., Whalley, L. K., Heard, D. E., Slater, E. J., Woodward-Massey, R., Ye,

677 C., Mehra, A., Worrall, S. D., Bacak, A., Coe, H., Percival, C. J., Hewitt, C. N., Lee, J.
678 D., Cui, T., Surratt, J. D., Wang, X., Lewis, A. C., Rickard, A. R., and Hamilton, J. F.:
679 Low-NO atmospheric oxidation pathways in a polluted megacity, *Atmos. Chem. Phys.*,
680 21, 1613-1625, 10.5194/acp-21-1613-2021, 2021.

681 Offenberg, J. H., Lewis, C. W., Lewandowski, M., Jaoui, M., Kleindienst, T. E., and Edney,
682 E. O.: Contributions of toluene and alpha-pinene to SOA formed in an irradiated
683 toluene/alpha-pinene/NO_x/air mixture: Comparison of results using C-14 content and
684 SOA organic tracer methods, *Environmental Science & Technology*, 41, 3972-3976,
685 10.1021/es070089+, 2007.

686 Offenberg, J. H., Lewandowski, M., Edney, E. O., Kleindienst, T. E., and Jaoui, M.: Influence
687 of Aerosol Acidity on the Formation of Secondary Organic Aerosol from Biogenic
688 Precursor Hydrocarbons, *Environmental Science & Technology*, 43, 7742-7747,
689 10.1021/es901538e, 2009.

690 Palmer, P. I., Marvin, M. R., Siddans, R., Kerridge, B. J., and Moore, D. P.: Nocturnal
691 survival of isoprene linked to formation of upper tropospheric organic aerosol, *Science*,
692 375, 562-566, doi:10.1126/science.abg4506, 2022.

693 Reid, J. P., Bertram, A. K., Topping, D. O., Laskin, A., Martin, S. T., Petters, M. D., Pope, F.
694 D., and Rovelli, G.: The viscosity of atmospherically relevant organic particles, *Nature*
695 *Communications*, 9, 10.1038/s41467-018-03027-z, 2018.

696 Riva, M., Budisulistiorini, S. H., Zhang, Z., Gold, A., and Surratt, J. D.: Chemical
697 characterization of secondary organic aerosol constituents from isoprene ozonolysis in
698 the presence of acidic aerosol, *Atmospheric Environment*, 130, 5-13,
699 10.1016/j.atmosenv.2015.06.027, 2016.

700 Rumsey, I. C., Cowen, K. A., Walker, J. T., Kelly, T. J., Hanft, E. A., Mishoe, K.,
701 Rogers, C., Proost, R., Beachley, G. M., Lear, G., Frelink, T., and Otjes, R. P.:
702 An assessment of the performance of the Monitor for AeRosols and GAses in
703 ambient air (MARGA): a semi-continuous method for soluble compounds,
704 *Atmos. Chem. Phys.*, 14, 5639-5658, 10.5194/acp-14-5639-2014, 2014.

705 Sarrafzadeh, M., Wildt, J., Pullinen, I., Springer, M., Kleist, E., Tillmann, R., Schmitt, S. H.,
706 Wu, C., Mentel, T. F., Zhao, D., Hastie, D. R., and Kiendler-Scharr, A.: Impact of NO_x
707 and OH on secondary organic aerosol formation from beta-pinene photooxidation,
708 *Atmospheric Chemistry and Physics*, 16, 11237-11248, 10.5194/acp-16-11237-2016,
709 2016.

710 Shrivastava, M., Cappa, C. D., Fan, J., Goldstein, A. H., Guenther, A. B., Jimenez, J. L.,
711 Kuang, C., Laskin, A., Martin, S. T., Ng, N. L., Petaja, T., Pierce, J. R., Rasch, P. J.,
712 Roldin, P., Seinfeld, J. H., Shilling, J., Smith, J. N., Thornton, J. A., Volkamer, R.,
713 Wang, J., Worsnop, D. R., Zaveri, R. A., Zelenyuk, A., and Zhang, Q.: Recent advances
714 in understanding secondary organic aerosol: Implications for global climate forcing,
715 *Reviews of Geophysics*, 55, 509-559, 10.1002/2016rg000540, 2017.

716 Shrivastava, M., Andreae, M. O., Artaxo, P., Barbosa, H. M. J., Berg, L. K., Brito, J., Ching,
717 J., Easter, R. C., Fan, J., Fast, J. D., Feng, Z., Fuentes, J. D., Glasius, M., Goldstein, A.
718 H., Alves, E. G., Gomes, H., Gu, D., Guenther, A., Jathar, S. H., Kim, S., Liu, Y., Lou,
719 S., Martin, S. T., McNeill, V. F., Medeiros, A., de Sa, S. S., Shilling, J. E., Springston, S.
720 R., Souza, R. A. F., Thornton, J. A., Isaacman-VanWertz, G., Yee, L. D., Ynoue, R.,
721 Zaveri, R. A., Zelenyuk, A., and Zhao, C.: Urban pollution greatly enhances formation of
722 natural aerosols over the Amazon rainforest, *Nature Communications*, 10,
723 10.1038/s41467-019-08909-4, 2019.

724 Song, M., Zhang, C., Wu, H., Mu, Y., Ma, Z., Zhang, Y., Liu, J., and Li, X.: The influence of
725 OH concentration on SOA formation from isoprene photooxidation, *Science of the Total*
726 *Environment*, 650, 951-957, 10.1016/j.scitotenv.2018.09.084, 2019.

727 Surratt, J. D., Lewandowski, M., Offenberg, J. H., Jaoui, M., Kleindienst, T. E., Edney, E. O.,
728 and Seinfeld, J. H.: Effect of acidity on secondary organic aerosol formation from

729 isoprene, *Environmental Science & Technology*, 41, 5363-5369, 10.1021/es0704176,
730 2007.

731 Surratt, J. D., Chan, A. W. H., Eddingsaas, N. C., Chan, M., Loza, C. L., Kwan, A. J., Hersey,
732 S. P., Flagan, R. C., Wennberg, P. O., and Seinfeld, J. H.: Reactive intermediates
733 revealed in secondary organic aerosol formation from isoprene, *Proceedings of the*
734 *National Academy of Sciences of the United States of America*, 107, 6640-6645,
735 10.1073/pnas.0911114107, 2010.

736 Wang, D. S., and Ruiz, L. H.: Secondary organic aerosol from chlorine-initiated oxidation of
737 isoprene, *Atmos. Chem. Phys.*, 17, 13491-13508, 10.5194/acp-17-13491-2017, 2017.

738 Wang, J., Ye, J., Zhang, Q., Zhao, J., Wu, Y., Li, J., Liu, D., Li, W., Zhang, Y., Wu, C., Xie,
739 C., Qin, Y., Lei, Y., Huang, X., Guo, J., Liu, P., Fu, P., Li, Y., Lee, H. C., Choi, H.,
740 Zhang, J., Liao, H., Chen, M., Sun, Y., Ge, X., Martin, S. T., and Jacob, D. J.: Aqueous
741 production of secondary organic aerosol from fossil-fuel emissions in winter Beijing
742 haze, *Proc Natl Acad Sci U S A*, 118, 10.1073/pnas.2022179118, 2021a.

743 Wang, J., Ye, J., Zhang, Q., Zhao, J., Wu, Y., Li, J., Liu, D., Li, W., Zhang, Y., Wu, C., Xie,
744 C., Qin, Y., Lei, Y., Huang, X., Guo, J., Liu, P., Fu, P., Li, Y., Lee, H. C., Choi, H.,
745 Zhang, J., Liao, H., Chen, M., Sun, Y., Ge, X., Martin, S. T., and Jacob, D. J.: Aqueous
746 production of secondary organic aerosol from fossil-fuel emissions in winter Beijing
747 haze, *Proceedings of the National Academy of Sciences of the United States of America*,
748 118, 10.1073/pnas.2022179118, 2021b.

749 Wang, S., Du, L., Tsona, N. T., Jiang, X., You, B., Xu, L., Yang, Z., and Wang, W.: Effect of
750 NO_x and SO₂ on the photooxidation of methylglyoxal: Implications in secondary
751 aerosol formation, *J Environ Sci (China)*, 92, 151-162, 10.1016/j.jes.2020.02.011, 2020.

752 Wang, X., Jacob, D. J., Downs, W., Zhai, S., Zhu, L., Shah, V., Holmes, C. D., Sherwen, T.,
753 Alexander, B., Evans, M. J., Eastham, S. D., Neuman, J. A., Veres, P. R., Koenig, T. K.,
754 Volkamer, R., Huey, L. G., Bannan, T. J., Percival, C. J., Lee, B. H., and Thornton, J. A.:
755 Global tropospheric halogen (Cl, Br, I) chemistry and its impact on oxidants, *Atmos.*
756 *Chem. Phys.*, 21, 13973-13996, 10.5194/acp-21-13973-2021, 2021c.

757 Wen, L., Chen, T., Zheng, P., Wu, L., Wang, X., Mellouki, A., Xue, L., and Wang, W.:
758 Nitrous acid in marine boundary layer over eastern Bohai Sea, China: Characteristics,
759 sources, and implications, *Sci. Total Environ.*, 10.1016/j.scitotenv.2019.03.225, 2019.

760 Wu, X., Xu, L. L., Hong, Y. W., Chen, J. F., Qiu, Y. Q., Hu, B. Y., Hong, Z. Y., Zhang, Y.
761 R., Liu, T. T., Chen, Y. T., Bian, Y. H., Zhao, G. Q., Chen, J. S., and Li, M. R.: The air
762 pollution governed by subtropical high in a coastal city in Southeast China: Formation
763 processes and influencing mechanisms, *Science of the Total Environment*, 692, 1135-
764 1145, 10.1016/j.scitotenv.2019.07.341, 2019.

765 Wu, X., Li, M., Chen, J., Wang, H., Xu, L., Hong, Y., Zhao, G., Hu, B., Zhang, Y., Dan, Y.,
766 and Yu, S.: The characteristics of air pollution induced by the quasi-stationary front:
767 Formation processes and influencing factors, *Science of the Total Environment*, 707,
768 10.1016/j.scitotenv.2019.136194, 2020.

769 Xiao, Y., Wu, Z., Guo, S., He, L., Huang, X., and Hu, M.: Formation mechanism of
770 secondary organic aerosol in aerosol liquid water: A review, *Chinese Science Bulletin*,
771 65, 3118-3133, 2020.

772 Xu, L., Du, L., Tsona, N. T., and Ge, M. F.: Anthropogenic Effects on Biogenic Secondary
773 Organic Aerosol Formation, *Advances in Atmospheric Sciences*, 38, 1053-1084,
774 10.1007/s00376-020-0284-3, 2021.

775 Xu, L., Guo, H. Y., Boyd, C. M., Klein, M., Bougiatioti, A., Cerully, K. M., Hite, J. R.,
776 Isaacman-VanWertz, G., Kreisberg, N. M., Knote, C., Olson, K., Koss, A., Goldstein, A.
777 H., Hering, S. V., de Gouw, J., Baumann, K., Lee, S. H., Nenes, A., Weber, R. J., and
778 Ng, N. L.: Effects of anthropogenic emissions on aerosol formation from isoprene and
779 monoterpenes in the southeastern United States, *Proceedings of the National Academy of*
780 *Sciences of the United States of America*, 112, 37-42, 10.1073/pnas.1417609112, 2015.

781 Yang, W., Cao, J., Wu, Y., Kong, F., and Li, L.: Review on plant terpenoid emissions
782 worldwide and in China, *The Science of the total environment*, 787, 147454-147454,
783 10.1016/j.scitotenv.2021.147454, 2021.

784 Zhang, J., An, J., Qu, Y., Liu, X., and Chen, Y.: Impacts of potential HONO sources on the
785 concentrations of oxidants and secondary organic aerosols in the Beijing-Tianjin-Hebei
786 region of China, *Science of the Total Environment*, 647, 836-852,
787 10.1016/j.scitotenv.2018.08.030, 2019a.

788 Zhang, P., Chen, T., Liu, J., Liu, C., Ma, J., Ma, Q., Chu, B., and He, H.: Impacts of SO₂,
789 Relative Humidity, and Seed Acidity on Secondary Organic Aerosol Formation in the
790 Ozonolysis of Butyl Vinyl Ether, *Environmental Science & Technology*, 53, 8845-8853,
791 10.1021/acs.est.9b02702, 2019b.

792 Zhang, Y.-Q., Chen, D.-H., Ding, X., Li, J., Zhang, T., Wang, J.-Q., Cheng, Q., Jiang, H.,
793 Song, W., Ou, Y.-B., Ye, P.-L., Zhang, G., and Wang, X.-M.: Impact of anthropogenic
794 emissions on biogenic secondary organic aerosol: observation in the Pearl River Delta,
795 southern China, *Atmospheric Chemistry and Physics*, 19, 14403-14415, 10.5194/acp-19-
796 14403-2019, 2019c.

797 Zhang, Y., Chen, Y., Lei, Z., Olson, N. E., Riva, M., Koss, A. R., Zhang, Z., Gold, A., Jayne,
798 J. T., Worsnop, D. R., Onasch, T. B., Kroll, J. H., Turpin, B. J., Ault, A. P., and Surratt,
799 J. D.: Joint Impacts of Acidity and Viscosity on the Formation of Secondary Organic
800 Aerosol from Isoprene Epoxydiols (IEPDX) in Phase Separated Particles, *Acs Earth and
801 Space Chemistry*, 3, 2646-2658, 10.1021/acsearthspacechem.9b00209, 2019d.

802 Zhao, D. F., Schmitt, S. H., Wang, M. J., Acir, I. H., Tillmann, R., Tan, Z. F., Novelli, A.,
803 Fuchs, H., Pullinen, I., Wegener, R., Rohrer, F., Wildt, J., Kiendler-Scharr, A., Wahner,
804 A., and Mentel, T. F.: Effects of NO_x and SO₂ on the secondary organic aerosol
805 formation from photooxidation of alpha-pinene and limonene, *Atmospheric Chemistry
806 and Physics*, 18, 1611-1628, 10.5194/acp-18-1611-2018, 2018.

807 Zheng, G., Su, H., Wang, S., Andreae, M. O., Poschl, U., and Cheng, Y.: Multiphase buffer
808 theory explains contrasts in atmospheric aerosol acidity, *Science*, 369, 1374-+,
809 10.1126/science.aba3719, 2020.

810 Zhou, M., Zheng, G., Wang, H., Qiao, L., Zhu, S., Huang, D., An, J., Lou, S., Tao, S., Wang,
811 Q., Yan, R., Ma, Y., Chen, C., Cheng, Y., Su, H., and Huang, C.: Long-term trends and
812 drivers of aerosol pH in eastern China, *Atmos. Chem. Phys. Discuss.*, 2021, 1-21,
813 10.5194/acp-2021-455, 2021.

814 Zhu, J., Penner, J. E., Yu, F., Sillman, S., Andreae, M. O., and Coe, H.: Decrease in radiative
815 forcing by organic aerosol nucleation, climate, and land use change, *Nature
816 Communications*, 10, 10.1038/s41467-019-08407-7, 2019.

817

818

819